HHS Public Access

Author manuscript

J Med Chem. Author manuscript; available in PMC 2021 March 12.

Published in final edited form as:

J Med Chem. 2020 March 12; 63(5): 1964–1977. doi:10.1021/acs.jmedchem.9b01623.

Radiotracer Development for Bacterial Imaging

Filipa Mota, **Alvaro A. Ordonez**

Center for Infection and Inflammation Imaging Research, Center for Tuberculosis Research, and Department of Pediatrics, Johns Hopkins University School of Medicine, Baltimore, Maryland 21287, United States

George Firth,

School of Biomedical Engineering and Imaging Sciences, St. Thomas' Hospital, King's College London, London SE1 7EH, United Kingdom

Camilo A. Ruiz-Bedoya,

Center for Infection and Inflammation Imaging Research, Center for Tuberculosis Research, and Department of Pediatrics, Johns Hopkins University School of Medicine, Baltimore, Maryland 21287, United States

Michelle T. Ma,

School of Biomedical Engineering and Imaging Sciences, St. Thomas' Hospital, King's College London, London SE1 7EH, United Kingdom

Sanjay K. Jain

Center for Infection and Inflammation Imaging Research, Center for Tuberculosis Research, and Department of Pediatrics, Johns Hopkins University School of Medicine, Baltimore, Maryland 21287, United States

Abstract

Bacterial infections remain a major threat to humanity and are a leading cause of death and disability. Antimicrobial resistance has been declared as one of the top ten threats to human health by the World Health Organization, and new technologies are urgently needed for the early diagnosis and monitoring of deep-seated and complicated infections in hospitalized patients. This review summarizes the radiotracers as applied to imaging of bacterial infections. We summarize the recent progress in the development of pathogen-specific imaging and the application of radiotracers in understanding drug pharmacokinetics as well as the local biology at the infection sites. We also highlight the opportunities for medicinal chemists in radiotracer development for bacterial infections, with an emphasis on target selection and radiosynthetic approaches. Imaging of infections is an emerging field. Beyond clinical applications, these technologies could provide

Corresponding Authors: **Filipa Mota** – Center for Infection and Inflammation Imaging Research, Center for Tuberculosis Research, and Department of Pediatrics, Johns Hopkins University School of Medicine, Baltimore, Maryland 21287, United States; fmota2@jhmi.edu, **Sanjay K. Jain** – Center for Infection and Inflammation Imaging Research, Center for Tuberculosis Research, and Department of Pediatrics, Johns Hopkins University School of Medicine, Baltimore, Maryland 21287, United States; sjain5@jhmi.edu.

The authors declare the following competing financial interest(s): S.K.J. received consulting fees from Mediso Medical Imaging Systems Ltd., unrelated to this work. A.A.O. and S.K.J. are co-inventors on pending patent US20150250906A1 on bacteria-specific labeled substrates as imaging biomarkers, filed by Johns Hopkins University.

Complete contact information is available at: https://pubs.acs.org/10.1021/acs.jmedchem.9b01623

unique insights into disease pathogenesis and expedite bench-to-bedside translation of new therapeutics.

Graphical Abstract

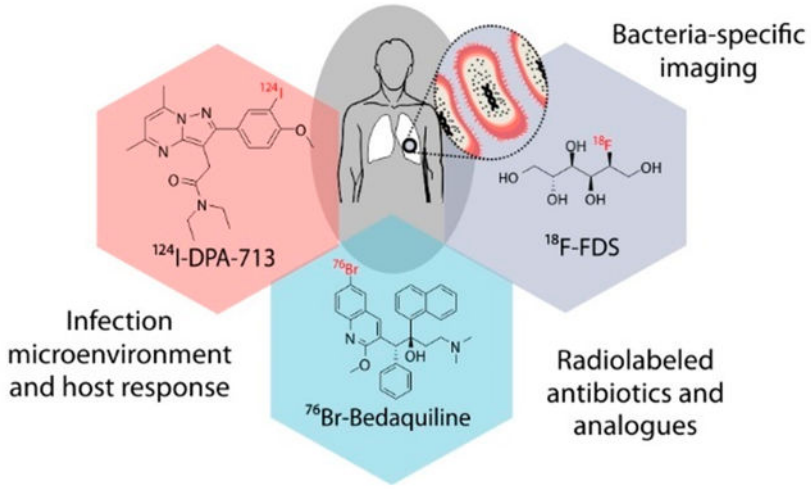

INTRODUCTION

While the discovery of penicillin marked a turning point in history, even ~100 years later, bacterial infections remain a major threat. The selection of antibiotic-resistant “super bugs” by the overuse of antibiotics and an increasingly susceptible patient population prone to life-threatening infections due to invasive procedures, implants, and cancer therapies remain as some of the major challenges in the field. In fact, antimicrobial resistance has been declared as one of the top ten threats to human health by the World Health Organization.[1] Therefore, the management of bacterial infections using safe, cheap, and plentiful antibiotics can no longer be taken for granted. It is estimated that by 2050, antibiotic-resistant infections will become the leading cause of death globally (10 million per year) and surpass those due to cancer.[2] Moreover, many of these patients have complex presentations with multiple different disease processes occurring simultaneously. Therefore, clinical and laboratory assessments do not always yield a clear etiology, which subsequently leads to delays in treatment or overuse of antibiotics. However, early detection and localization of infections in these patients could not only lead to rapid institution of appropriate antibiotic treatments but also avoid unnecessary treatments in those that do not have bacterial infections.

Traditional tools such as microscopy, microbiology, and molecular techniques including nucleic acid amplification and mass spectrometry, require clinical samples (blood, urine, stool, or cerebrospinal fluid) that may not accurately represent the biology at deep-seated infection sites and thus are often nondiagnostic.[3] Therefore, direct tissue sampling of the infection site by surgical resection or biopsy is often utilized to establish a definitive diagnosis. However, these invasive techniques are logistically challenging, costly, and often do not yield a diagnosis due to sampling error/bias. Furthermore, some fastidious bacteria such as *Mycobacterium tuberculosis* or anaerobes are difficult to cultivate ex vivo, which

can also limit or delay diagnosis. Currently available imaging tools such as radiography, ultrasonography, computed tomography (CT), and magnetic resonance imaging (MRI) are therefore often incorporated into the diagnostic workup. Because these techniques rely on anatomic changes that occur late in the disease process, they are nonspecific and cannot reliably differentiate infections from other disease processes such as malignancies or sterile inflammation.[3,4] More sensitive nuclear medicine techniques such as ^{111}In-oxine-tagged white blood cell γ-scintigraphy and 2-^{18}F-fluorodeoxyglucose (^{18}F-FDG) positron emission tomography (PET), are also nonspecific and dependent upon host immune responses to infection, which may be altered in immunosuppressed patients most at risk for infections. Therefore, there is a need for rapid, whole body, noninvasive imaging that could specifically detect and localize sites of infection and also provide a readout on the disease burden. Molecular imaging could complement traditional clinical tools especially when available clinical samples would be insensitive, high risk, or impractical (e.g., biopsy for brain infection). Pathogen-specific imaging could be used to rapidly diagnose deep-seated infections due to multidrug or antibiotic-resistant (MDR) bacteria, where the risks (and costs) of empiric second- or third-line antibiotic treatment are high and for immunocompromised patients (e.g., fever and neutropenia due to cancer chemotherapy, organ transplant) who are high-risk populations and for whom routine imaging to detect infections is already an established clinical practice. Molecular imaging tools could also help in establishing end points in patients requiring prolonged antibiotic duration (months-year) and could be especially useful for patients with implants and foreign bodies for which current imaging tools are inadequate and nonspecific.

PET and single-photon emission tomography (SPECT) imaging are molecular imaging tools that have been extensively applied in oncology, neurology, and other fields, with similar potential for infections. Combined with CT or MRI for anatomical reference, these hybrid tools (PET/CT, SPECT/CT, PET/MRI) allow the direct noninvasive visualization of molecular biology in vivo. In this review, we highlight how selective metabolism of small molecules by bacteria can be exploited to develop radiotracers for clinical applications to specifically detect and localize bacterial infections. We review the application of radiochemistry to understand antimicrobial pharmacokinetics (PK) in situ, as well as radiotracers designed to study local biology in vivo. Recent developments in the design, radiosynthesis, and applications of radiotracers in this field are described. Furthermore, we propose opportunities for the design, discovery, and development of pathogen-specific radiotracers by medicinal chemists, especially in the fields of antimicrobial drug discovery and molecular imaging.

PATHOGEN-SPECIFIC IMAGING

Target Selection.

While molecular imaging in oncology aims to differentiate neoplastic cells with minor variations from other eukaryotic cells from the same lineage, bacteria-specific radiotracers take advantage of the significant structural and metabolic differences of prokaryotes. Until recently, target selection has mainly focused on antibiotics, which while highly specific, target and kill (or disable) bacteria at high potency. Therefore, many radiolabeled antibiotics

may not be ideal candidates for bacteria-specific imaging unless they are accumulated by bacteria many orders of magnitude greater than by mammalian tissues.[5] More recent efforts for developing pathogen-specific imaging agents target specific bacterial pathways, including the metabolism of carbohydrates, bacterial folate biosynthesis, and iron transport systems unique to bacteria, components of and selective binders to the bacterial cell wall, substrates for intracellular bacterial proteins, and antimicrobial peptides (Figure 1).[6,7] The main advantage of this approach is signal amplification due to enzymatic turnover or retention within the bacteria, which can be detected by imaging over the background signal from uninfected mammalian tissues.

Selected pathogen-specific radiotracers described in the following sections have been summarized in Table 1.

Carbohydrate Metabolism.— ^{18}F-FDG is the most commonly used diagnostic PET radiotracer for clinical oncology and infectious diseases, making fluoride-18 (^{18}F, half-life = 110 min, β^+ 96.9%, E_{max} = 634 keV[26]) the most widely used radioisotope.[27] As an analogue of glucose, ^{18}F-FDG accumulates in cells with increased glycolysis regardless of the cause leading to this metabolic change. Therefore, ^{18}F-FDG is not capable of distinguishing between infection and sterile processes (e.g., neoplasia, autoimmune disorders, etc.). While glucose is metabolized by most organisms, some sugars are only metabolized by bacteria. Through a systematic screening of small molecules, Ordonez and Weinstein et al. reported that the sorbitol analogue 2-^{18}F-fluorodeoxysorbitol (^{18}F-FDS) is metabolized selectively by Enterobacterales (*Escherichia coli*, *Klebsiella* sp., *Enterobacter* sp., *Salmonella* sp., etc.), a group of rod-shaped Gram-negative bacteria that are the most common cause of bacterial infections in humans.[7] ^{18}F-FDS is conveniently synthesized by a simple reduction of ^{18}F-FDG with sodium borohydride (Figure 2A).[28] The maltose–maltodextrin transporter internalizes α-1,4-linked glucose oligomers (maltodextrins) as a source of glucose and is only functional in metabolically active bacteria. Ning et al. developed ^{18}F-maltohexaose (MH^{18}F) as a radiotracer that could potentially image bacteria with specificity, although there was high background signal.[11] Because the transporter recognizes the nonreducing end of maltodextrins (i.e., the end that does not have a free aldehyde or ketone group), the reducing end of maltohexaose was functionalized to undergo nucleophilic substitution (S_N2) by ^{18}F-fluoride (Figure 2B).[11] Maltose is a disaccharide formed of two glucose units joined by a glycosidic link between the α-anomeric form of C1 in one sugar and the hydroxyl oxygen atom on C4 of the other. Two radiofluorinated analogues of maltose have been reported in which the ^{18}F-label is located either at the 1- or 6- positions in a single unit. 6-^{18}F-Fluoromaltose is prepared by nucleophilic displacement of a nosylate group by ^{18}F-fluoride, followed by hydrolysis of the acetyl-protecting groups. The analogue 1-^{18}F-fluoromaltose that has been synthesized by nucleophilic displacement of the triflate-substituted precursor, however, proved unstable upon purification. 6-^{18}F-Fluoromaltose was also able to distinguish infection from sterile inflammation in vivo, although high background tissue retention was observed,[29] leading to the development of the second-generation analogue 6″-^{18}F-fluoromaltotriose (Figure 2C).[12] While targeting the maltose–maltodextrin transporter is a promising approach, the presence of starch-degrading enzymes

in blood requires special attention in the design of these radiotracers to avoid in vivo degradation.[30]

Folate Metabolism.—While humans can only acquire folic acid through their diet, most bacteria require de novo synthesis. This metabolic distinction in folate biosynthesis has been explored as a target for antibiotics, such as sulfonamides, which act as competitive inhibitors of bacterial dihydropteroate synthase (DHPS). DHPS catalyzes the incorporation of *para*-aminobenzoic acid (PABA) into tetrahydrofolate.[15] Mammals, however, lack the machinery to utilize PABA and rapidly eliminate it through urinary excretion. PABA and its antibacterial structural analogue, sulfonamide, enter bacterial cells by passive diffusion through nonspecific porin channels. ^{3}H-PABA was found to accumulate in bacteria following a small molecule screening, and it was subsequently developed as a PET radiotracer using carbon-11 (^{11}C, half-life = 20.4 min, β^+ 99.8%, E_{max} = 960 keV[26]).[7] ^{11}C-PABA was synthesized via cyclotron generated $^{11}CO_2$ and a commercially available Grignard precursor (Figure 3A).[32] In a mouse model of *E. coli* infection, the uptake of ^{11}C-PABA in infected tissue was 2.6-fold higher than in the inflamed control tissue inoculated with heat-killed bacteria.[13] The PABA analogue 2-fluoro-PABA was found to be a suitable alternative substrate for tetrahydrofolate and was subsequently developed as a radiotracer using ^{18}F. 2-^{18}F-PABA was obtained in three steps by conventional nucleophilic aromatic substitution radiofluorination of the commercially available precursor 2,4-dinitrolzenzonitrile (Figure 3B).[15] Sellmyer et al. developed a radiotracer based on the broad-spectrum antibiotic trimethoprim (TMP), which inhibits bacterial dihydrofolate reductase, an enzyme in the DNA synthesis and folate pathway that is conserved across most bacterial species. TMP has a higher affinity for the bacterial target compared to the human equivalent and the radiotracer design was based on reported structure–activity relationships of TMP analogues. ^{18}F-Fluoropropyl-trimethoprim (^{18}F-FPTMP) is prepared by S_N2 radiofluorination in a one-pot two-step protocol (Figure 3C).[16]

Iron Metabolism (Siderophores).—Iron (Fe) is an essential micronutrient for bacteria and fungi to survive and replicate. Bacteria and fungi biosynthesize and secrete specific chelators, termed siderophores, that sequester Fe^{3+} from the surrounding environment. The resulting Fe^{3+} complexes are highly stable and are recognized and taken up by active transporters of the microorganism. Many siderophores are specific to particular species or categories of bacteria. The metal ion Ga^{3+} possesses the same charge and a similar ionic radius to high spin Fe^{3+}. As a result, it exhibits similar coordination properties and also forms highly stable siderophore complexes. Active transporters involved in the uptake of Fe^{3+}-siderophore complexes do not sufficiently distinguish the Fe^{3+} siderophore complex from the respective Ga^{3+} complex and therefore can also take up the complementary Ga^{3+}-bound siderophore. Recent research has exploited this, and a library of siderophores have been radiolabeled with the PET isotope gallium-68 (^{68}Ga, half-life = 67.7 min, β^+ 88.9%, E_{max} = 1899 keV[26]) and screened for uptake first in rodent models of *Aspergillus fumigatus* fungal infections and also in bacteria. ^{67}Ga (half-life = 78 h, EC) is a γ-emitting isotope used in γ-scintigraphy/SPECT imaging, and formulations of ^{67}Ga, most notably citrate formulations, have historically been used for imaging infection, as well as inflammation.[33,34] The ability of $^{67/68}Ga^{3+}$ to image infection is likely due to its tendency to behave

similarly to Fe^{3+}. Citrate has a modest affinity for Ga^{3+} (log β_1 = 10.02), and thus $^{67/68}Ga^{3+}$ may dissociate in vivo from citrate. The free $^{67/68}Ga^{3+}$ can be sequestered by pathogenic organisms via siderophores. Alternatively, ^{68}Ga-citrate or the dissociated $^{67/68}Ga^{3+}$ is sequestered by host inflammatory cells[35] and therefore cannot always distinguish inflammation from infection.[6] More recently, $^{68}Ga^{3+}$ complex of pyoverdine PAO1 (PVD–PAO1), a siderophore produced by *Pseudomonas aeruginosa*, was developed via generator-produced ^{68}Ga. PET studies using a murine *P. aeruginosa* infection model have shown specific accumulation of ^{68}Ga-PVD–PAO1 in infected tissues versus ^{18}F-FDG or ^{68}Ga-citrate (Figure 4).[17]

Nucleic Acids.—Anaerobic bacteria have been explored as tumor-killing toxins due to their ability to proliferate in hypoxic areas. A strain of *Clostridium novyi*-NT (C. *novyi*-NT) that lacks its lethal toxin has been engineered and shown to have promise as a bacterial-based cancer therapeutic agent.[36] With the aim of monitoring this therapy in vivo, a SPECT radiotracer targeting bacterial thymidine kinase (TK) was developed. 1-(2′-Deoxy-2′-fluoro-β-D-arabinofuranosyl)-5-iodoracil (FIAU) is a thymidine nucleoside analogue and a substrate for TK in a variety of bacteria, which upon phosphorylation becomes intracellularly trapped. The SPECT radiotracer 125I-FIAU showed in vivo uptake in *E. coli*, *S. aureus*, *E. faecalis*, and *C. novyi*-NT bacterial strains. On the basis of these findings, a PET analogue containing iodine-124 (^{124}I, half-life = 4.2 days, β^+ 22.7%, E_{max} = 2138 keV[26]), ^{124}IFIAU, initially developed as an imaging agent for viral infections,[37] was studied in patients with musculoskeletal infections, where it demonstrated positive signal in the sites of infection. The radiosynthesis of ^{124}I-FIAU proceeds by the radioiodination of 1-(2′-deoxy-1-β-D-arabinofuranosyl)-uracil with ^{124}I-NaI (Figure 5A).

Bacterial-Specific Cell Wall Components.—Most bacteria produce and incorporate D-amino acids into their cell walls, a process that is absent in mammalian cells. Neumann et al. reported the radiolabeling and characterization of D-methyl-^{11}C-methionine (^{11}C-D-Met). The radiosynthetic strategy for ^{11}C-D-Met was based on an automated method developed for ^{11}C-L-Met and consists of the methylation of a D-homocysteinethiolactone with gas phase produced $^{11}CH_3I$ (Figure 5B). In vivo, ^{11}C-D-Met selectively differentiates both *E. coli* and *S. aureus* infections from sterile inflammation.[20]

Antimicrobial peptides can be endogenously generated by cells involved in the host immune response. The cationic peptide ubiquicidin (UBI) is present in the human respiratory epithelium and preferentially binds to the negatively charged bacterial cell wall.[38] Several ^{99m}Tc-radiolabeled peptidic fragments of UBI showed increased sensitivity and selectivity for bacteria and ^{99m}Tc-UBI-29–41 showed promise for SPECT imaging of several bacterial strains in preclinical and clinical studies.[39–41] An ^{18}F-labeled analogue of ^{99m}Tc-UBI-29–41 was developed, but its use was limited by defluorination in vivo.[42] Vilche et al. developed a ^{68}Ga-analogue using a NOTA ligand (Figure 5C), and first-in-human studies have been reported.[23]

Although many pathogen-specific targets have been explored, some have proved more successful than others. For example, while several studies utilizing radiolabeled antibiotics have been published, they are not in use clinically.[5] This is likely, as some radiolabeled

antibiotics may not be ideal candidates for imaging unless the mechanism of bacterial accumulation is orders of magnitude greater for the bacteria than for human tissues.[38,43] While several clinical studies utilizing antimicrobial peptides have been reported, and some antimicrobial peptides have shown promise for specific detection of bacterial infections (e.g., Sathekge et al. using ^{99m}Tc-UBI-29–41),[41] they have not yet been widely accepted for pathogen-specific imaging. Similarly, despite its initial promise, clinical studies utilizing ^{124}I-FIAU PET reported low specificity and poor imaging quality in patients with suspected prosthetic joint infections,[19] due to muscle uptake possibly due to FIAU metabolism by human mitochondrial TK2.[44] Finally, some bacteria-specific radiotracers are dependent on the metabolic state of the bacteria or on bacterial growth and multiplication.[7] Therefore, at a low metabolic state and slow growth rate, the incorporation of some radiotracers might not be sufficient for high signal-to-noise ratios. Conversely, some radiotracers such as ^{11}C-PABA seem to be independent of the bacterial metabolic state and thus have the potential to detect slowly dividing bacteria.[7] Ideally, the target would be highly conserved and specific for bacteria and the radiotracer would be able to accumulate in both susceptible and drug-resistant organisms at different growth phases. From a molecular design standpoint, however, there is not a mathematical algorithm that would allow us to predict such characteristics. Nonetheless, on the basis of the development history of the radiotracers reviewed here, we can devise key considerations for de novo design of pathogen-specific small molecule PET imaging agents, as summarized in Figure 6.

Compound Screening and Structural Design.

Once a target has been identified, the discovery of new “leads” may follow a conventional compound screen, structure-based design, or optimization of molecular probes developed for other imaging techniques such as fluorescence. Unbiased screening approaches are necessary for the discovery of novel candidates that could be developed as pathogen-specific imaging agents. While screening random libraries of radiolabeled compounds has yielded promising results,[7] another approach would be to explore the vast existing libraries of antibiotic analogues developed by medicinal chemists. Many analogues which may not have high potency and are thus discarded for the purposes of developing antibiotics could nonetheless be developed as promising pathogen-specific imaging agents. Specifically, examination of their structure–activity/binding relationships and selection of compounds with very high affinity to bacterial targets and the potential for accumulation would be ideal. When optimizing the chemical structure of the desired radiotracer, the structural motif of the molecule required for bacterial recognition and specificity must be kept intact while other components can ideally be explored for radiolabeling and optimization of physicochemical properties. Screening of bacteria-specific radiotracer candidates should be performed in whole bacterial cell cultures because the fact that a probe can selectively bind an essential bacterial enzyme does not mean it can also penetrate the bacterial cell wall or be successfully delivered to the sites of infection.[4]

Choice of Radiolabel.

A crucial factor for the development of new radiotracers is the introduction of the radiolabel itself, which can substantially alter the chemical properties and bacterial uptake of the tracer. Whether the radiotracer in question is a radiolabeled version of a known biologically

relevant molecule or a novel compound designed to be an imaging agent, addition of a radiolabel may significantly impact its behavior in vivo. ^{99m}Tc is widely used in SPECT imaging due to its low cost, 6 h half-life that allows it to be shipped, and ease of radiolabeling. Because it is a radiometal, the incorporation of ^{99m}Tc into molecules occurs through chelation, either through a ligand linked to the target molecule or through direct chelation with the pharmacophore of interest. Although this allows for straightforward kit-based radiolabeling, it may affect several properties of the molecule being radiolabeled, particularly if direct chelation is taking place, as the functional groups required for chelation may also be crucial for the binding or solvation of the molecule. Covalent binding of PET isotopes circumvents these limitations, albeit with additional constraints. For instance, the main advantage of radiolabeling with ^{11}C is that it allows the chemical structure of the target molecule to remain unchanged, which is critical when performing PK analysis of radiolabeled antibiotics (e.g., ^{11}C-rifampin). ^{11}C is also the radiolabel of choice for amino acids and derivatives (e.g., ^{11}C-D-Met). However, while ^{11}C provides excellent image quality, its 20 min half-life limits its use due to the need for an on-site high energy cyclotron. Furthermore, if the radiotracer is expected to take several hours to accumulate inside the bacteria, a short-lived isotope such as ^{11}C might is not ideal. ^{18}F is the most commonly used PET radioisotope, providing high quality images and allowing imaging for up to 5 h post injection. Accordingly, the majority of bacteria-specific PET radiotracers in development are radiofluorinated, either because they derive from widely available ^{18}F-FDG (e.g., ^{18}F-FDS) or because they have been designed to incorporate ^{18}F (e.g., ^{18}F-FPTMP). Because ^{18}F-fluoride can be produced by low energy cyclotrons in high quantities and shipped to other locations, it offers several advantages over ^{11}C. The limitations of ^{18}F come from the complexity of chemistry required for radiolabeling and rather common radiotracer defluorination in vivo. ^{124}I has a 4-day half-life, which is very useful for molecules with long biological half-lives such as antibodies, although the images generated are poor because only 23% of its decay is through positron emission. In addition, in vivo deiodination can also occur and lead to toxicity. As in ^{99m}Tc SPECT imaging, PET radiometals can also be incorporated through chelation to a ligand that is in turn covalently linked to the target molecule. While this can significantly change the physicochemical properties of small molecules and in vivo PK, it can also be exploited as a way to transport and deposit radiometals into bacteria. For example, siderophores act themselves as the metal chelator (e.g., ^{68}Ga-PVD–PAO1), and large antimicrobial peptides (e.g., ^{68}Ga-NOTA–UBI-29–41), which bind to extracellular targets, are less affected by the bulky metal–chelator complex. ^{68}Ga can be easily obtained from a benchtop generator and allows very simple radiosynthesis, but this is also a limitation because its short half-life of 68 min and low amounts of activity generated prevent it from being shipped to remote locations. An alternative to ^{68}Ga is the SPECT isotope ^{67}Ga with a 3 day half-life. Other PET radiometals of notable mention are zirconium-89 (^{89}Zr, half-life = 3.3 days, β^+ 22.7%, E_{max} = 902 keV[26]) and copper-64 (^{64}Cu, half-life = 12.7 h, β^+ 38.5%, E_{max} = 653 keV[26]), although these have not been vastly used in PET imaging of bacterial infections.

Physicochemical Predictors.

The structural design, inclusive of radiolabel choice as mentioned above, must be an iterative process that takes into consideration in silico predictors and in vitro characterization of

physicochemical properties. Lipophilicity, polar surface area, and net charge are properties that can influence the radiotracer's ability to penetrate the blood–brain barrier and other target tissues where infected lesions are present. From several PK studies performed with radiolabeled antibiotics, we know that delivery to sites where bacteria reside is often low due the poor vascularization and presence of necrotic tissue as well as high cellular density. Highly lipophilic small molecules often show high plasma protein binding and slow clearance rate, and positively charged, hydrophilic radiotracers are rapidly cleared by the kidneys. Thus, when analyzing a library of potential radiotracers, one should take into consideration not only their in vitro cellular uptake but also their physicochemical properties.

Synthetic Strategy and Radiochemistry.

Due to the half-life constraint of most PET isotopes as well as high energy exposure to the chemist, fast, simple, and reproducible radiolabeling strategies are usually sought. Precursors of very high purity are required, and a synthetic route that allows late stage radiolabeling in one or two steps is preferred. A key difference between radiochemistry and standard synthetic chemistry is the scale of the reaction, as most radiosynthesis will use subpicomolar concentrations of radioisotope. The identity of the resulting compound must be easily confirmed, which is commonly achieved by HPLC. Because in most cases the radiotracer must be obtained on the same day as the PET imaging, it is imperative that radiosynthesis, purification, and quality control are optimized and a balance between radiochemical yield, time of preparation, and starting amounts of radioactivity is achieved. The formulation of the radiotracer is also important, and stability should be measured early on.

Clinical Translation.

Assuming a promising new radiotracer has been discovered and characterized in small animal molecules, its synthesis must be optimized for good manufacturing practice (GMP) standard production before it can be translated into humans. Early stage radiosynthesis is often performed manually or in automated radiosynthesis modules in a radiochemistry lab. For complicated radiosynthesis, manual handling allows complex multistep protocols to be followed, but the use of automated systems strongly decreases the radiation exposure of the radiochemist. When translating the protocols into a clinical PET center, however, other factors must be taken into considerations in order to comply with the guidelines stipulated by the respective regulatory agency.[45]

RADIOLABELED ANTIBIOTICS AND ANALOGUES TO STUDY DRUG BIODISTRIBUTION

The discovery and development of highly effective and safe antimicrobials presents additional challenges to the conventional drug development pipeline. At the early stages of drug discovery, antimicrobial efficacy is determined by the susceptibility of the microorganism to the antimicrobial using the minimum inhibitory concentration (MIC). However, effective treatment of infections depends on achieving adequate antibiotic concentrations at infection sites, where the pathogen resides.[46] While drug dosing is

commonly determined by PK studies based on drug concentration in plasma, this traditional approach provides inconsistent information regarding drug delivery and biodistribution in different organs or areas. Reduced penetration of antibiotics into privileged infected sites such as necrotic pulmonary tissues or infections localized in the brain can lead to their poor performance. PET imaging can provide a multicompartment dynamic profile of the radiolabeled antibiotic in vivo noninvasively. A major challenge with radiolabeled antibiotics is to find radiochemistry conditions that allow the incorporation of a radioisotope that results in a radiotracer chemically identical to the parent drug. Additionally, matching the physical half-life of the radioisotope with the biological half-life of the drug is important. In some cases, an analogue of the drug can be used as a surrogate if its behavior in vivo mimics that of the drug. A major advantage of this technology is clinical translatability and the ability to measure PK simultaneously in multiple organs/tissue compartments with relatively unaltered physiology. Therefore, these studies could provide detailed PK data in humans and enable phase 0 clinical studies, typically small studies of 10–20 patients,[47] that are strongly encouraged by the FDA for new drug applications.[48]

Antimycobacterials.

The front-line antimicrobials used for the treatment of tuberculosis (TB) are isoniazid, pyrazinamide, and rifampin, and they have all been radiolabeled with ^{11}C, thus retaining their chemical identity. ^{11}C-isoniazid can be synthesized in a three-step one-pot reaction from ^{11}C-HCN and iodopyridine (Figure 7A).[49] Amartey et al. developed a fluorinated analogue of isoniazid, 2-^{18}F-fluoroisoniazid, which can be obtained from a trimethylammonium precursor in two steps (Figure 7B).[50] In 2012, Weinstein et al. reported the PK of 2-^{18}F-fluoroisoniazid in *Mycobacterium tuberculosis*-infected mice, where it accumulated in the lungs of infected animals compared to healthy controls and showed that the fluorinated analogue, which requires specific activation for accumulation within the bacteria, mimics the behavior of isoniazid.[51] Although a similar approach was followed to obtain ^{11}C-pyrazinamide and its fluorinated analogue, 5-^{18}F-fluoropyrazinamide was found not to be a substrate for the *M. tuberculosis* PZase enzyme and therefore it does not mimic the behavior of the drug in vivo.[49,52] Rifampin is a semisynthetic macrocycle derived from the natural product rifamycin, and it acts by inhibiting bacterial DNA polymerase. Rifampin was originally radiolabeled by *N*-methylation at the piperazine moiety with $^{11}CH_3I$ (Figure 7C), and a different synthesis using ^{11}C-methyl triflate as the starting material has also been reported.[49,53] In a rabbit model of tuberculous (TB) meningitis, Tucker et al. noted that penetration of ^{11}C-rifampin in the brain is limited, heterogeneous, and varies as the treatment progresses.[54] First-in-human ^{11}C-rifampin PET in patients with pulmonary TB[55] and one patient with TB meningitis[54] demonstrated limited pulmonary cavitary and brain penetration of the radiolabeled drug, respectively. Bedaquiline, a bromine-containing diarylquinoline, inhibits the mycobacterial ATP synthase and offers synergy with both first- and second-line TB drugs. It received accelerated FDA approval in 2012.[56] Recently, the radiolabeling of bedaquiline with bromine-76 (^{76}Br, half-life = 16.2 h, β^+ 54.8%, E_{max} = 3382 keV[26]) to generate a radiotracer identical to the parent compound was reported (Figure 7D).[57] PET imaging in a mouse model of pulmonary TB showed ^{76}Br-bedaquiline selectively localizes in adipose tissue, has excellent penetration into infected lung lesions, and (previously unreported) measurable uptake in the brain parenchyma.[57]

Broad-Spectrum Antibiotics.

Fluoroquinolones are a class of broad-spectrum antibiotics which exhibit concentration-dependent bactericidal activity by inhibiting enzymes essential for bacterial DNA replication. While this section discusses the use of radiolabeled antibiotics and analogs to study drug biodistribution, it should be noted that in the 1990s, an analogue of ciprofloxacin labeled with ^{99m}Tc was commercialized as a bacteria-specific SPECT imaging agent. However, lack of specificity was subsequently reported.[58–61] Because fluoroquinolones contain at least one fluorine atom, this facilitated their development into ^{18}F-labeled PET radiotracers. The radiolabeling of ciprofloxacin has been reported by ^{19}F–^{18}F isotopic exchange, a method that has been applied to radiolabel other fluoroquinolones,[62,63] although it is rarely considered for radiotracer development as it is lengthy (approximately 40 min) and usually leads to low yields and specific activity.[64] Langer et al. reported that direct isotopic exchange on ciprofloxacin itself was unsuccessful and developed a two-step synthetic strategy starting with a 7-chloro-substituted precursor (Figure 8A).[65] Fleroxacin has a fluoroethyl substituent, which allows for a different type of radiolabeling strategy to be employed. Livni et al. report the radiosynthesis of ^{18}F-fleroxacin from a mesylate precursor by standard S_N2 radiofluorination (Figure 8B).[66]

IMAGING THE MICROENVIRONMENT

Infectious lesions are characterized by a heterogeneous microenvironment, which may include spatial physical and chemical differences as well as varied immune responses. While our current understanding of the local biology at the sites of infection derives from molecular biology techniques performed on resected tissues, in vivo PET imaging performed with radiotracers targeted at inflammation biomarkers may provide valuable information regarding the heterogeneity of infection sites and help in developing novel host-directed therapies (Figure 9). For example, the potential of hypoxia imaging has been evaluated in pulmonary TB, which is characterized by hypoxic caseous granulomas and with hypoxia being a determinant of bacterial persistence.[67,68] In a mouse model of pulmonary tuberculosis, copper(II)-diacetyl-bis(*N*4-methylthiosemicarbazone) (^{64}Cu-ATSM) showed progressive time-dependent accumulation in tuberculous lesions.[69] An alternative PET radiotracer for hypoxia imaging is ^{18}F-fluoromisonidazole, ^{18}F-FMISO, which has been clinically used to characterize tissue hypoxia in TB patients, where it accumulates in regions of TB consolidation and around pulmonary cavities.[70] Reactive oxygen and nitrogen species, collectively referred to as ROS, are endogenously generated by the mitochondria and are essential to normal cell function. When ROS are excessively generated, however, this may result in DNA and protein oxidation and ultimately lead to cell death.[71] Oxidative stress is considered a hallmark of inflammation and has also been used as the target for therapeutics.[72] ^{18}F-ROStrace was evaluated in a mouse model of lipopolysaccharide (LPS)-induced neuroinflammation characterized by superoxide generation[73] and showed significantly higher uptake in LPS-treated animals. Because LPS is a major component of the outer surface membrane present in almost all Gram-negative bacteria, and ROS have been proposed to play critical roles in microbial metabolism,[74,75] we hypothesize there is potential for PET imaging of oxidative stress in bacterial infections. ^{64}Cu-LLP2A is an imaging agent used for PET imaging of melanoma and other tumors expressing very late

Ag-4 (VLA-4). Identifying the cell types present in these lesions may allow a more precise host-directed treatment targeting. Mattila et al. tested the VLA-4-targeting peptidomimetic ^{64}Cu-LLP2A in macaques with TB and found that the radiotracer retention was driven by macrophages and T cells in TB granulomas.[76] The translocator protein (TSPO) has been extensively targeted for imaging of neuroinflammation under several pathologies.[77,78] In the context on infection, Foss et al. developed a SPECT analogue, ^{125}I-DPA-713.[79] This tracer was used to monitor TB treatments in animal models and provide early readouts on the efficacy of novel TB treatments.[80] In humans, the PET analogue ^{124}I-DPA-713 was safe and well tolerated, showing rapid clearance from the lungs in healthy volunteers, and thus has potential for use in humans for diseases with macrophage-associated inflammation (e.g., TB, sarcoid, inflammatory bowel disease).[81] ^{68}Ga-Pentixafor was developed based on a small cyclic peptide, which is an inverse agonist of the chemokine receptor CXCR4.[82] Following its evaluation in several cancers, and due to the role of CXCR4 in inflammatory responses and high expression levels in lymphocytes, ^{68}Ga-Pentixafor was recently evaluated in 14 patients with suspected bone infections. Eight out of nine patients with positive ^{68}Ga-Pentixafor had pathology-confirmed infections.[83]

CONCLUSIONS

Molecular imaging for infectious diseases is an emerging field with tremendous potential for both preclinical and clinical applications. Although several targets and screening approaches have been explored, this field would get a major boost from unbiased screens to identify novel biological targets and chemical leads. Some of the major challenges in this field have been highlighted and could be overcome by applying existing medicinal chemistry resources and approaches. Sustained, multidisciplinary efforts are needed in this field.

ACKNOWLEDGMENTS

This work was funded by the NIH: Director’s Transformative Research Award R01-EB020539, R01-HL131829, R01-EB025985, and R56-AI145435 to S.K.J. and the Department of Defense’s Congressionally Directed Medical Research Programs PR-171338P1 to S.K.J.

Biographies

Filipa Mota completed her Ph.D. in chemical biology and medicinal chemistry in 2014 from University College London, after which she joined a biotech as a medicinal chemist. Under the mentorship of Professor David Selwood, Filipa designed and developed small molecule tools and new technologies to study biological systems. During her postdoctoral work at King’s College London, she undertook training in molecular imaging and led the development of new small molecule radiotracers for oxidative stress. Filipa is currently a research fellow at Johns Hopkins School of Medicine, focusing on radiotracer design and development for bacterial imaging.

Alvaro A. Ordonez completed his medical studies at the Universidad Industrial de Santander in Bucaramanga, Colombia. As a postdoctoral fellow at the Johns Hopkins School of Medicine under the guidance of Dr. Sanjay Jain, he led the discovery, characterization,

and clinical translation of multiple bacteria-specific imaging tracers. He is now an assistant professor in the Department of Pediatrics at the Johns Hopkins School of Medicine.

George Firth obtained his M.Sc. in biological sciences from the University of Hull in 2017. Alongside his supervisor Dr. Graeme J. Stasiuk, he designed novel zinc sensing probes for prostate cancer. He developed a keen interest in the development of imaging probes and their transition from a chemistry-based environment to a biological one. He is currently a Ph.D. student at King's College London, working under the supervision of Professor Philip J. Blower, using positron emission tomography to benefit the field of metallomics.

Camilo A. Ruiz-Bedoya obtained his M.D. from Pontificia Universidad Javeriana in Bogota, Colombia, where he also conducted research in obesity and diabetes. During his rotation at Johns Hopkins School of Medicine, he focused on new molecular imaging techniques for renal imaging. Camilo is currently a research fellow at Johns Hopkins School of Medicine, where he is developing new animal models of infectious diseases and taking part in clinical studies evaluating new radiotracers for positron emission tomography imaging of tuberculosis.

Michelle T. Ma started out in chemistry at the University of Queensland, where she completed a B.Sc. with Honours. She first became interested in radionuclide imaging chemistry during her Ph.D., at the University of Melbourne, working for Paul Donnelly on chelators for the PET radioisotope, copper-64. She is now a senior lecturer in imaging chemistry at King's College London. Her group's research encompasses radio, chelator, imaging, and bioconjugate chemistry.

Sanjay K. Jain received his medical degree in 1999 from the All India Institute of Medical Sciences in New Delhi. He trained in pediatrics at Penn State Children's Hospital, Milton S. Hershey Medical Center, and the Tufts University School of Medicine. He was a clinical fellow in pediatric infectious diseases and is currently a Professor of Pediatrics, Radiology & Radiological Sciences and International Health at the Johns Hopkins University. He directs the Center for Infection and Inflammation Imaging Research and the Pediatric Infectious Diseases fellowship program and is a member of the Center for TB Research at Johns Hopkins.. His primary research interests include the development of novel imaging technologies for bacterial infections, pediatric tuberculosis (TB), and TB meningitis.

ABBREVIATIONS USED

PET	positron emission tomography
^{18}F-FDG	^{18}F-fluorodeoxyglucose
^{18}F-FDS	2-^{18}F-fluorodeoxysorbitol
MH^{18}F	^{18}F-maltohexaose
DCY	decay-corrected yield
F-2-FDTre	deoxyfluoro-D-trehalose

NDCY	nondecay corrected yield
PABA	para-aminobenzoic acid
DHPS	dihydropteroate
TMP	trimethoprim
^{18}F-FPTMP	^{18}F-fluoropropyl-trimetho-prim
^{11}C-D-Met	D-methyl-^{11}C-methionine
TK	thymidine kinase
FIAU	1-(2′-deoxy-2′-fluoro-β-D-arabinofuranosyl)-5-iodoracil
UBI	ubiquicidin
MIC	minimum inhibitory concentration
TB	tuberculosis
INH	Isoniazid
PZA	pyrazinamode
RIF	rifampin
TBM	tuberculous meningitis
Cu-BTSC	copper(II) bis(thiosemicarbazone) complex
ROS	reactive oxygen species
LPS	lipopolysaccharide

REFERENCES

(1). Ten Threats to Global Health in 2019; World Health Organization, 2019; https://www.who.int/emergencies/ten-threats-to-global-health-in-2019 (accessed Jan 6, 2020).

(2). O'Neill J Tackling Drug-Resistant Infections Globally: Final Report and Recommendations; Review on Antimicrobial Resistance; Wellcome Trust and UK Government, 2016; https://amr-review.org/sites/default/files/160525_Final%20paper_with%20cover.pdf (accessed Dec 30, 2019).

(3). Jain SK The promise of molecular imaging in the study and treatment of infectious diseases. Mol. Imaging Biol 2017, 19 (3), 341–347. [PubMed: 28155078]

(4). Ordonez AA; Sellmyer MA; Gowrishankar G; Ruiz-Bedoya CA; Tucker EW; Palestro CJ; Hammoud DA; Jain SK Molecular imaging of bacterial infections: Overcoming the barriers to clinical translation. Sci. Transl. Med 2019, 11 (508), No. eaax8251.

(5). Lucignani G The many roads to infection imaging. Eur. J. Nucl. Med. Mol. Imaging 2007, 34 (11), 1873–1877. [PubMed: 17786435]

(6). Ordonez AA; Jain SK Pathogen-specific bacterial imaging in nuclear medicine. Semin. Nucl. Med 2018, 48 (2), 182–194. [PubMed: 29452620]

(7). Ordonez AA; Weinstein EA; Bambarger LE; Saini V; Chang YS; DeMarco VP; Klunk MH; Urbanowski ME; Moulton KL; Murawski AM; Pokkali S; Kalinda AS; Jain SK A systematic

approach for developing bacteria-specific imaging tracers. J. Nucl. Med 2017, 58 (1), 144–150. [PubMed: 27635025]

(8). Weinstein EA; Ordonez AA; DeMarco VP; Murawski AM; Pokkali S; MacDonald EM; Klunk M; Mease RC; Pomper MG; Jain SK Imaging Enterobacteriaceae infection in vivo with 18F-fluorodeoxysorbitol positron emission tomography. Sci. Transl. Med 2014, 6 (259), 259ra146.

(9). Zhu W; Yao S; Xing H; Zhang H; Tai YC; Zhang Y; Liu Y; Ma Y; Wu C; Wang H; Li Z; Wu Z; Zhu Z; Li F; Huo L Biodistribution and radiation dosimetry of the Enterobacteriaceae-specific imaging probe [(18)F]fluorodeoxysorbitol determined by PET/CT in healthy human volunteers. Mol. Imaging Biol 2016, 18(5), 782–787. [PubMed: 27020679]

(10). Ordonez AA; Granados U; Wintaco LM; Ruiz-Bedoya CA; Frey S; Sanchez JD; D'Alessio FR; Holt DP; Dannals RF; Pomper MG; Jain SK Noninvasive Diagnosis and Monitoring of Pulmonary Infections using Pathogen-Specific 18F-fluorodeoxysorbitol (18F-FDS) PET—First in Human Study. In Proceedings of the World Molecular Imaging Conference, Montreal, QC, Canada, 4–7 Sep 2019; World Molecular Imaging Society, 2019; Abstr GA 321.

(11). Ning X; Seo W; Lee S; Takemiya K; Rafi M; Feng X; Weiss D; Wang X; Williams L; Camp VM; Eugene M; Taylor WR; Goodman M; Murthy N PET imaging of bacterial infections with fluorine-18-labeled maltohexaose. Angew. Chem., Int. Ed 2014, 53 (51), 14096–14101.

(12). Gowrishankar G; Hardy J; Wardak M; Namavari M; Reeves RE; Neofytou E; Srinivasan A; Wu JC; Contag CH; Gambhir SS Specific imaging of bacterial infection using 6"-18F-fluoromaltotriose: a second-generation PET tracer targeting the maltodextrin transporter in bacteria. J. Nucl. Med 2017, 58 (10), 1679–1684. [PubMed: 28490473]

(13). Mutch CA; Ordonez AA; Qin H; Parker M; Bambarger LE; Villanueva-Meyer JE; Blecha J; Carroll V; Taglang C; Flavell R; Sriram R; VanBrocklin H; Rosenberg O; Ohliger MA; Jain SK; Neumann KD; Wilson DM [11C] Paraaminobenzoic acid: a positron emission tomography tracer targeting bacteria-specific metabolism. ACS Infect. Dis 2018, 4 (7), 1067–1072. [PubMed: 29712422]

(14). Ordonez AA; Ruiz-Bedoya CA; Plyku D; Klunk MH; Holt DP; Dannals RF; Wilson DM; Jain SK, Noninvasive Imaging of Infections Using 11C-para-Aminobenzoic Acid (11C-PABA) as a Bacteria-Specific PET Radiotracer: Preclinical and First-in-Human Studies. In Proceedings of the World Molecular Imaging Conference, Montreal, QC, Canada, 4–7 Sep 2019; World Molecular Imaging Society, 2019; Abstr P051.

(15). Zhang Z; Ordonez AA; Wang H; Li Y; Gogarty KR; Weinstein EA; Daryaee F; Merino J; Yoon GE; Kalinda AS; Mease RC; Iuliano JN; Smith-Jones PM; Jain SK; Tonge PJ Positron emission tomography imaging with 2-[18F] F-p-aminobenzoic acid detects Staphylococcus aureus infections and monitors drug response. ACS Infect. Dis 2018, 4 (11), 1635–1644. [PubMed: 30067329]

(16). Sellmyer MA; Lee I; Hou C; Weng C-C; Li S; Lieberman BP; Zeng C; Mankoff DA; Mach RH Bacterial infection imaging with [18F]fluoropropyl-trimethoprim. Proc. Natl. Acad. Sci. U. S. A 2017, 114 (31), 8372–8377. [PubMed: 28716936]

(17). Petrik M; Umlaufova E; Raclavsky V; Palyzova A; Havlicek V; Haas H; Novy Z; Dolezal D; Hajduch M; Decristoforo C Imaging of Pseudomonas aeruginosa infection with Ga-68 labelled pyoverdine for positron emission tomography. Sci. Rep 2018, 8, 15698. [PubMed: 30356077]

(18). Diaz LA Jr.; Foss CA; Thornton K; Nimmagadda S; Endres CJ; Uzuner O; Seyler TM; Ulrich SD; Conway J; Bettegowda C; Agrawal N; Cheong I; Zhang X; Ladenson PW; Vogelstein BN; Mont MA; Zhou S; Kinzler KW; Vogelstein B; Pomper MG Imaging of musculoskeletal bacterial infections by [124I]FIAU-PET/CT. PLoS One 2007, 2 (10), No. e1007. [PubMed: 17925855]

(19). Zhang XM; Zhang HH; McLeroth P; Berkowitz RD; Mont MA; Stabin MG; Siegel BA; Alavi A; Barnett TM; Gelb J; Petit C; Spaltro J; Cho SY; Pomper MG; Conklin JJ; Bettegowda C; Saha S [124I]FIAU: Human dosimetry and infection imaging in patients with suspected prosthetic joint infection. Nucl. Med. Biol 2016, 43 (5), 273–279. [PubMed: 27150029]

(20). Neumann KD; Villanueva-Meyer JE; Mutch CA; Flavell RR; Blecha JE; Kwak T; Sriram R; VanBrocklin HF; Rosenberg OS; Ohliger MA; Wilson DM Imaging active infection in vivo using d-amino acid derived pet radiotracers. Sci. Rep 2017, 7, 7903. [PubMed: 28801560]

(21). Stewart MN; Parker MF; Jivan S; Luu JM; Huynh TL; Schulte B; Seo Y; Blecha JE; Villanueva-Meyer JE; Flavell RR; VanBrocklin HF; Ohliger MA; Rosenberg O; Wilson DM High

enantiomeric excess in-loop synthesis of d-[methyl-11C] methionine for use as a diagnostic positron emission tomography radiotracer in bacterial infection. ACS Infect. Dis 2020, 6, 43–49.

(22). Vilche M; Reyes AL; Vasilskis E; Oliver P; Balter H; Engler H 68Ga-NOTA-UBI-29–41 as a PET tracer for detection of bacterial nfection. J. Nucl. Med 2016, 57 (4), 622–627. [PubMed: 26769861]

(23). Ebenhan T; Sathekge M; Lengana T; Koole M; Gheysens O; Govender T; Zeevaart JR 68Ga-NOTA-functionalized ubiquicidin: cytotoxicity, biodistribution, radiation dosimetry and first-in-human positron emission tomography/computed tomography imaging of infections. J. Nucl. Med 2018, 59, 334–339. [PubMed: 29051342]

(24). Bhusari P; Bhatt J; Sood A; Kaur R; Vatsa R; Rastogi A; Mukherjee A; Dash A; Mittal BR; Shukla J Evaluating the potential of kit-based 68Ga-ubiquicidin formulation in diagnosis of infection: a pilot study. Nucl. Med. Commun 2019, 40 (3), 228–234. [PubMed: 30480552]

(25). Nazari B; Azizmohammadi Z; Rajaei M; Karami M; Javadi H; Assadi M; Asli IN Role of 99mTc-ubiquicidin 29–41 scintigraphy to monitor antibiotic therapy in patients with orthopedic infection: a preliminary study. Nucl. Med. Commun 2011, 32 (8), 745–751. [PubMed: 21659909]

(26). Conti M; Eriksson L Physics of pure and non-pure positron emitters for PET: a review and a discussion. EJNMMI Phys 2016, 3,8. [PubMed: 27271304]

(27). Lawal I; Zeevaart JR; Ebenhan T; Ankrah A; Vorster M; Kruger H; Govender T; Sathekge M Metabolic imaging of infection. J. Nucl. Med 2017, 58 (11), 1727–1732. [PubMed: 28818989]

(28). Li Z-B; Wu Z; Cao Q; Dick DW; Tseng JR; Gambhir SS; Chen X The synthesis of 18F-FDS and its potential application in molecular imaging. Mol. Imaging. Biol 2008, 10 (2), 92–98. [PubMed: 18097725]

(29). Gowrishankar G; Namavari M; Jouannot EB; Hoehne A; Reeves R; Hardy J; Gambhir SS Investigation of 6-[18F]-fluoromaltose as a novel PET tracer for imaging bacterial infection. PLoS One 2014, 9 (9), No. e107951. [PubMed: 25243851]

(30). Axer A; Hermann S; Kehr G; Clases D; Karst U; Fischer-Riepe L; Roth J; Fobker M; Schäfers M; Gilmour R; Faust A Harnessing the maltodextrin transport mechanism for targeted bacterial imaging: structural requirements for improved in vivo stability in tracer design. ChemMedChem 2018, 13, 241–250. [PubMed: 29195027]

(31). Ning X; Seo W; Lee S; Takemiya K; Rafi M; Feng X; Weiss D; Wang X; Williams L; Camp VM; Eugene M; Taylor WR; Goodman M; Murthy N Fluorine-18 labeled maltohexaose images bacterial infections by PET. Angew. Chem., Int. Ed 2014, 53, 14096–14101.

(32). Holt DP; Kalinda AS; Bambarger LE; Jain SK; Dannals RF Radiosynthesis and validation of [Carboxy-11C] 4-A minobenzoic acid ([11 C] PABA), a PET radiotracer for imaging bacterial infections. J. Labelled Compd. Radiopharm 2019, 62 (1), 28–33.

(33). Palestro CJ The current role of gallium imaging in infection. Semin. Nucl. Med 1994, 24 (2), 128–141. [PubMed: 8023169]

(34). Vorster M; Maes A; van de Wiele C; Sathekge M 68Gacitrate PET/CT in Tuberculosis: a pilot study. Q. J. Nucl. Med. Mol. Imaging 2019, 63, 48–55. [PubMed: 24651268]

(35). Hoffer PB; Huberty J; Khayam-Bashi H The association of Ga-67 and lactoferrin. J. Nucl. Med 1977, 18 (7), 713–717. [PubMed: 267143]

(36). Dang LH; Bettegowda C; Huso DL; Kinzler KW; Vogelstein B Combination bacteriolytic therapy for the treatment of experimental tumors. Proc. Natl. Acad. Sci. U. S. A 2001, 98 (26), 15155–15160. [PubMed: 11724950]

(37). Jacobs A; Bräunlich I; Graf R; Lercher M; Sakaki T; Voges J; Hesselmann V; Brandau W; Wienhard K; Heiss W-D Quantitative kinetics of [124I] FIAU in cat and man. J. Nucl. Med 2001, 42 (3), 467–475. [PubMed: 11337525]

(38). Lupetti A; Welling MM; Pauwels EK; Nibbering PH Radiolabelled antimicrobial peptides for infection detection. Lancet Infect. Dis 2003, 3 (4), 223–229. [PubMed: 12679265]

(39). Ferro-Flores G; Arteaga de Murphy C; Pedraza-López M; Meléndez-Alafort L; Zhang Y-M; Rusckowski M; Hnatowich DJ In vitro and in vivo assessment of 99m Tc-UBI specificity for bacteria. Nucl. Med. Biol 2003, 30, 597–603. [PubMed: 12900285]

(40). Akhtar MS; Qaisar A; Irfanullah J; Iqbal J; Khan B; Jehangir M; Nadeem MA; Khan MA; Afzal MS; Imran MB Antimicrobial peptide 99mTc-ubiquicidin 29–41 as human infection-imaging agent: clinical trial. J. Nucl. Med 2005, 46 (4), 567–573. [PubMed: 15809477]

(41). Sathekge M; Garcia-Perez O; Paez D; El-Haj N; Kain-Godoy T; Lawal I; Estrada-Lobato E Molecular imaging in musculoskeletal infections with 99m Tc-UBI 29–41 SPECT/CT. Ann. Nucl. Med 2018, 32 (1), 54–59. [PubMed: 29164482]

(42). Salber D; Gunawan J; Langen K-J; Fricke E; Klauth P; Burchert W; Zijlstra S Comparison of 99mTc-and 18F-ubiquicidin autoradiography to anti–Staphylococcus aureus immunofluorescence in rat muscle abscesses. J. Nucl. Med 2008, 49 (6), 995–999. [PubMed: 18483088]

(43). Welling M; Stokkel M; Balter J; Sarda-Mantel L; Meulemans A; Le Guludec D The many roads to infection imaging. Eur. J. Nucl. Med. Mol. Imaging 2008, 35 (4), 848–849.

(44). Wang L; Munch-Petersen B; Herrstrom Sjoberg A; Hellman U; Bergman T; Jornvall H; Eriksson S Human thymidine kinase 2: molecular cloning and characterisation of the enzyme activity with antiviral and cytostatic nucleoside substrates. FEBS Lett 1999, 443 (2), 170–174. [PubMed: 9989599]

(45). Schwarz SW; Decristoforo C; Goodbody AE; Singhal N; Saliba S; Ruddock PS; Zukotynski K; Ross AA Harmonization of US, European Union, and Canadian first-in-human regulatory requirements for radiopharmaceuticals: is this possible? J. Nucl. Med 2019, 60 (2), 158–166.

(46). Ehrlich P Chemotherapeutics: scientific principles, methods and results. Address in pathology to 17th International Congress of Medicine. Lancet 1913, 182 (4694), 445–451.

(47). Rubinstein LV; Steinberg SM; Kummar S; Kinders R; Parchment RE; Murgo AJ; Tomaszewski JE; Doroshow JH The statistics of phase 0 trials. Stat. Med 2010, 29 (10), 1072–1076. [PubMed: 20419759]

(48). Guidance for Industry and Researchers: the Radioactive Drug Research Committee: Human Research Without an Investigational New Drug Application; U.S. Food and Drug Administration, 2009); http://www.fda.gov/downloads/Drugs/Guidances/UCM163892.pdf.

(49). Liu L; Xu Y; Shea C; Fowler JS; Hooker JM; Tonge PJ Radiosynthesis and bioimaging of the tuberculosis chemotherapeutics isoniazid, rifampicin and pyrazinamide in baboons. J. Med. Chem 2010, 53 (7), 2882–2891. [PubMed: 20205479]

(50). Amartey JK; Esguerra C; Al-Otaibi B; Parhar RS; Al-Jammaz I 2-[(18)F]-fluoroisonicotinic acid hydrazide: biological evaluation in an acute infection model. Appl. Radiat. Isot 2004, 60(6), 839–843. [PubMed: 15110348]

(51). Weinstein E; Liu L; Ordonez AA; Wang H; Hooker JM; Tonge P; Jain SK Noninvasive determination of 2-[18F]-fluoroisonicotinic acid hydrazide pharmacokinetics by positron emission tomography in Mycobacterium tuberculosis-infected mice. Antimicrob. Agents Chemother 2012, 56 (12), 6284–6290. [PubMed: 23006755]

(52). Zhang Z; Ordonez AA; Smith-Jones P; Wang H; Gogarty KR; Daryaee F; Bambarger LE; Chang YS; Jain SK; Tonge PJ The biodistribution of 5-[18F]fluoropyrazinamide in Mycobacterium tuberculosis-infected mice determined by positron emission tomography. PLoS One 2017, 12 (2), No. e0170871. [PubMed: 28151985]

(53). DeMarco VP; Ordonez AA; Klunk M; Prideaux B; Wang H; Zhuo Z; Tonge PJ; Dannals RF; Holt DP; Lee CK; Weinstein EA; Dartois V; Dooley KE; Jain SK Determination of [11C] rifampin pharmacokinetics within Mycobacterium tuberculosis-infected mice by using dynamic positron emission tomography bioimaging. Antimicrob. Agents Chemother 2015, 59 (9), 5768–5774. [PubMed: 26169396]

(54). Tucker EW; Guglieri-Lopez B; Ordonez AA; Ritchie B; Klunk MH; Sharma R; Chang YS; Sanchez-Bautista J; Frey S; Lodge MA; Rowe SP; Holt DP; Gobburu JVS; Peloquin CA; Mathews WB; Dannals RF; Pardo CA; Kannan S; Ivaturi VD; Jain SK Noninvasive (11)C-rifampin positron emission tomography reveals drug biodistribution in tuberculous meningitis. Sci. Transl. Med 2018, 10 (470), No. eaau0965. [PubMed: 30518610]

(55). Ordonez AA; Wang H; Magombedze G; Ruiz-Bedoya CA; Srivastava S; Chen A; Tucker EW; Urbanowski ME; Pieterse L; Cardozo EF; Lodge MA; Shah MR; Holt DP; Mathews WB; Dannals RF; Gobburu JVS; Peloquin CA; Rowe SP; Gumbo T; Ivaturi VD; Jain SK Dynamic

imaging in tuberculosis patients reveals heterogeneous drug exposures in pulmonary lesions. Nat. Med 2020, DOI: 10.1038/s41591-020-0770-2.

(56). Cox E; Laessig K FDA approval of bedaquiline—the benefit–risk balance for drug-resistant tuberculosis. N. Engl. J. Med 2014, 371 (8), 689–691. [PubMed: 25140952]

(57). Ordonez AA; Carroll LS; Abhishek S; Mota F; Ruiz-Bedoya CA; Klunk MH; Singh AK; Freundlich JS; Mease RC; Jain SK Radiosynthesis and PET bioimaging of (76)Br-Bedaquiline in a murine model of tuberculosis. ACS Infect. Dis 2019, 5 (12), 1996–2002. [PubMed: 31345032]

(58). Siaens RH; Rennen HJ; Boerman OC; Dierckx R; Slegers G Synthesis and comparison of 99mTc-enrofloxacin and 99mTc-ciprofloxacin. J. Nucl. Med 2004, 45 (12), 2088–2094. [PubMed: 15585486]

(59). Vinjamuri S; Hall AV; Solanki KK; Bomanji J; Siraj Q; O'Shaughnessy E; Das SS; Britton KE Comparison of 99mTc infecton imaging with radiolabelled white-cell imaging in the evaluation of bacterial infection. Lancet 1996, 347 (8996), 233–235. [PubMed: 8551884]

(60). Solanki K; Bomanji J; Siraj Q; Small M; Britton K Tc-99m Infecton: a new class of radiopharmaceutical for imaging infection. J. Nucl. Med 1993, 34 (5), 119.

(61). Britton KE; Wareham DW; Das SS; Solanki KK; Amaral H; Bhatnagar A; Katamihardja AHS; Malamitsi J; Moustafa HM; Soroa VE; Sundram FX; Padhy AK Imaging bacterial infection with 99mTc-ciprofloxacin (Infecton). J. Clin. Pathol 2002, 55 (11), 817–823. [PubMed: 12401818]

(62). Fischman AJ; Babich JW; Alpert NM; Vincent J; Wilkinson RA; Callahan RJ; Correia JA; Rubin RH Pharmacokinetics of 18F-labeled trovafloxacin in normal and Escherichia coli-infected rats and rabbits studied with positron emission tomography. Clin. Microbiol. Infect 1997, 3 (1), 63–72. [PubMed: 11864078]

(63). Tewson T; Yang D; Wong G; Macy D; DeJesus O; Nickles R; Perlman S; Taylor M; Frank P The synthesis of fluorine-18 lomefloxacin and its preliminary use in human studies. Nucl. Med. Biol 1996, 23 (6), 767–772. [PubMed: 8940719]

(64). Langer O; Mitterhauser M; Wadsak W; Brunner M; Müller U; Kletter K; Müller M A general method for the fluorine-18 labelling of fluoroquinolone antibiotics. J. Labelled Compd. Radiopharm 2003, 46 (8), 715–727.

(65). Langer O; Mitterhauser M; Brunner M; Zeitlinger M; Wadsak W; Mayer BX; Kletter K; Müller M Synthesis of fluorine-18-labeled ciprofloxacin for PET studies in humans. Nucl. Med. Biol 2003, 30 (3), 285–291. [PubMed: 12745020]

(66). Livni E; Babich J; Alpert NM; Liu Y-Y; Thom E; Cleeland R; Prosser BL; Correia JA; Strauss HW; Rubin RH; Fischman AJ Synthesis and biodistribution of 18F-labeled fleroxacin. Nucl. Med. Biol 1993, 20, 81–87. [PubMed: 8461883]

(67). Krohn KA; Link JM; Mason RP Molecular imaging of hypoxia. J. Nucl. Med 2008, 49 (2), 129S–148S. [PubMed: 18523070]

(68). Via LE; Lin PL; Ray SM; Carrillo J; Allen SS; Eum SY; Taylor K; Klein E; Manjunatha U; Gonzales J; Lee EG; Park SK; Raleigh JA; Cho SN; McMurray DN; Flynn JL; Barry CE III Tuberculous granulomas are hypoxic in guinea pigs, rabbits, and nonhuman primates. Infect. Immun 2008, 76 (6), 2333–2340. [PubMed: 18347040]

(69). Harper J; Skerry C; Davis SL; Tasneen R; Weir M; Kramnik I; Bishai WR; Pomper MG; Nuermberger EL; Jain SK Mouse model of necrotic tuberculosis granulomas develops hypoxic lesions. J. Infect. Dis 2012, 205 (4), 595–602. [PubMed: 22198962]

(70). Belton M; Brilha S; Manavaki R; Mauri F; Nijran K; Hong YT; Patel NH; Dembek M; Tezera L; Green J; Moores R; Aigbirhio F; Al-Nahhas A; Fryer TD; Elkington PT; Friedland JS Hypoxia and tissue destruction in pulmonary TB. Thorax 2016, 71 (12), 1145–1153. [PubMed: 27245780]

(71). Sies H; Berndt C; Jones DP Oxidative stress. Annu. Rev. Biochem 2017, 86, 715–748. [PubMed: 28441057]

(72). Halasi M; Wang M; Chavan TS; Gaponenko V; Hay N; Gartel AL ROS inhibitor N-acetyl-L-cysteine antagonizes the activity of proteasome inhibitors. Biochem. J 2013, 454 (2), 201–208. [PubMed: 23772801]

(73). Hsu H-Y; Wen M-H Lipopolysaccharide-mediated reactive oxygen species and signal transduction in the regulation of interleukin-1 gene expression. J. Biol. Chem 2002, 277 (25), 22131–22139. [PubMed: 11940570]

(74). McBee ME; Chionh YH; Sharaf ML; Ho P; Cai MW; Dedon PC Production of superoxide in bacteria is stress-and cell state-dependent: A gating-optimized flow cytometry method that minimizes ROS measurement artifacts with fluorescent dyes. Front. Microbiol 2017, 8, 459. [PubMed: 28377755]

(75). Alexander C; Rietschel ET Bacterial lipopolysaccharides and innate immunity. J. Endotoxin Res 2001, 7, 167–202. [PubMed: 11581570]

(76). Mattila JT; Beaino W; Maiello P; Coleman MT; White AG; Scanga CA; Flynn JL; Anderson CJ Positron emission tomography imaging of macaques with tuberculosis identifies temporal changes in granuloma glucose metabolism and integrin $\alpha 4\beta 1$–expressing immune cells. J. Immunol 2017, 199 (2), 806–815. [PubMed: 28592427]

(77). Werry EL; Bright FM; Piguet O; Ittner LM; Halliday GM; Hodges JR; Kiernan MC; Loy CT; Kril JJ; Kassiou M Recent developments in TSPO PET imaging as a biomarker of neuroinflammation in neurodegenerative disorders. Int. J. Mol. Sci 2019, 20 (13), 3161.

(78). Herrera-Rivero M; Heneka MT; Papadopoulos V Translocator protein and new targets for neuroinflammation. Clin. Transl. Imaging 2015, 3 (6), 391–402.

(79). Foss CA; Harper JS; Wang H; Pomper MG; Jain SK Noninvasive molecular imaging of tuberculosis-associated inflammation with radioiodinated DPA-713. J. Infect. Dis 2013, 208 (12), 2067–2074. [PubMed: 23901092]

(80). Ordonez AA; Pokkali S; DeMarco VP; Klunk M; Mease RC; Foss CA; Pomper MG; Jain SK Radioiodinated DPA-713 imaging correlates with bactericidal activity of tuberculosis treatments in mice. Antimicrob. Agents Chemother 2015, 59 (1), 642–649. [PubMed: 25403669]

(81). Foss CA; Plyku D; Ordonez AA; Sanchez-Bautista J; Rosenthal HB; Minn I; Lodge MA; Pomper MG; Sgouros G; Jain SK Biodistribution and radiation dosimetry of 124I-DPA-713, a PET radiotracer for macrophage-associated inflammation. J. Nucl. Med 2018, 59 (11), 1751–1756. [PubMed: 29700124]

(82). Demmer O; Gourni E; Schumacher U; Kessler H; Wester HJ PET imaging of CXCR4 receptors in cancer by a new optimized ligand. ChemMedChem 2011, 6 (10), 1789–1791. [PubMed: 21780290]

(83). Bouter C; Meller B; Sahlmann CO; Staab W; Wester HJ; Kropf S; Meller J 68Ga-Pentixafor PET/CT imaging of chemokine receptor CXCR4 in chronic infection of the bone: first insights. J. Nucl. Med 2018, 59 (2), 320–326. [PubMed: 28729430]

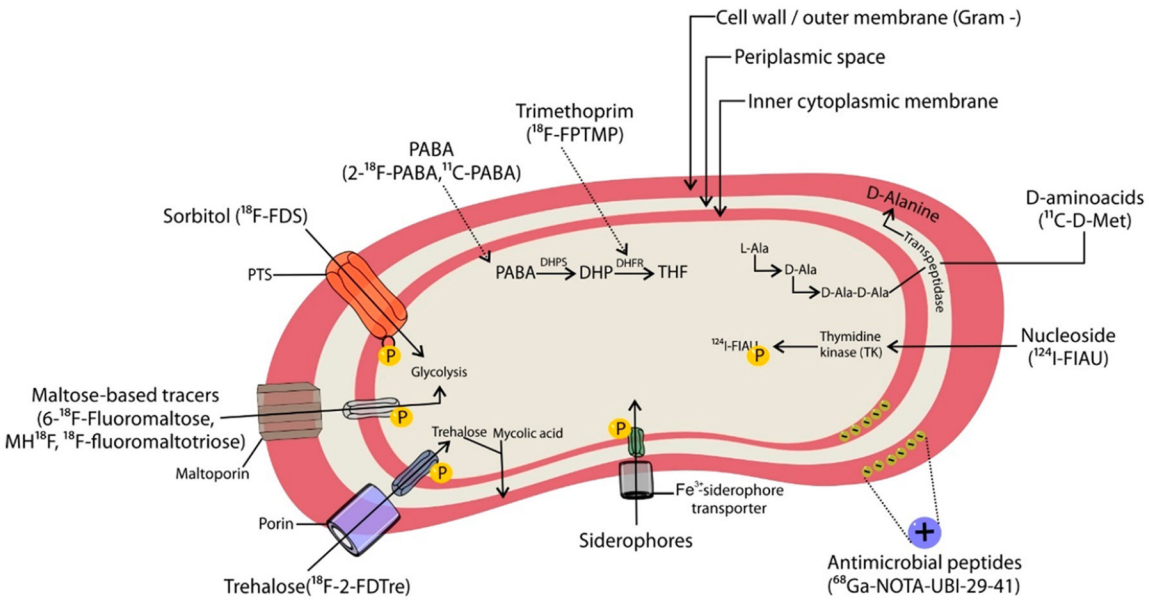

Figure 1.

Molecular targets for bacteria-specific imaging agents. PTS, phosphotransferase system; DHPS, dihydropteroate synthetase; DHP, dihydrofolic acid; THF, tetrahydrofolic acid.

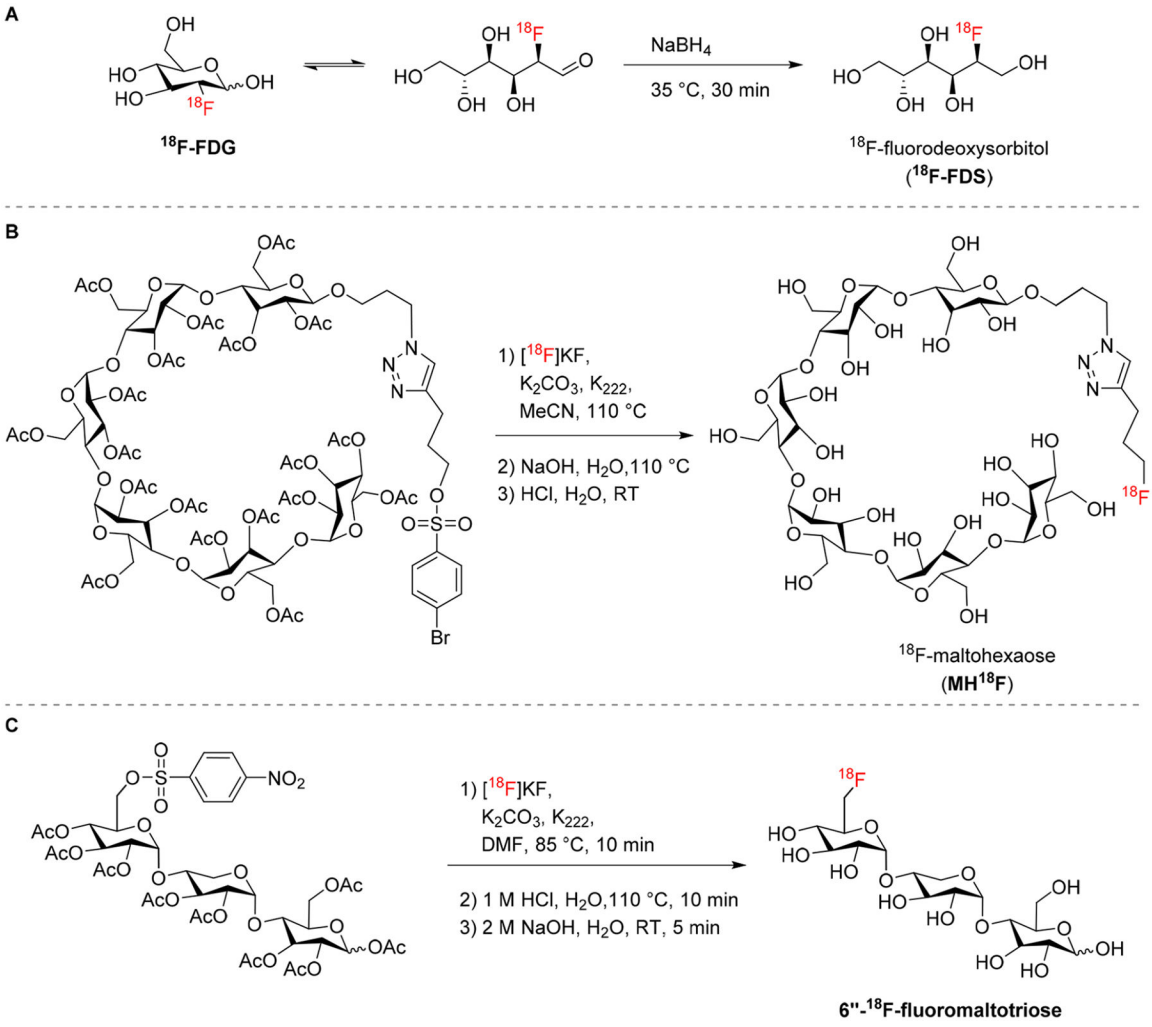

Figure 2.

Radiosynthesis of sugar-based radiotracers used in bacterial imaging. (A) ^{18}F-FDS is obtained from reduction of ^{18}F-FDG.[28] (B) MH^{18}F and (C) 6″-^{18}F-fluoromaltotriose are radiolabeled by nucleophilic substitution with ^{18}F-fluoride, followed by deprotection of the hydroxyl groups.12,31

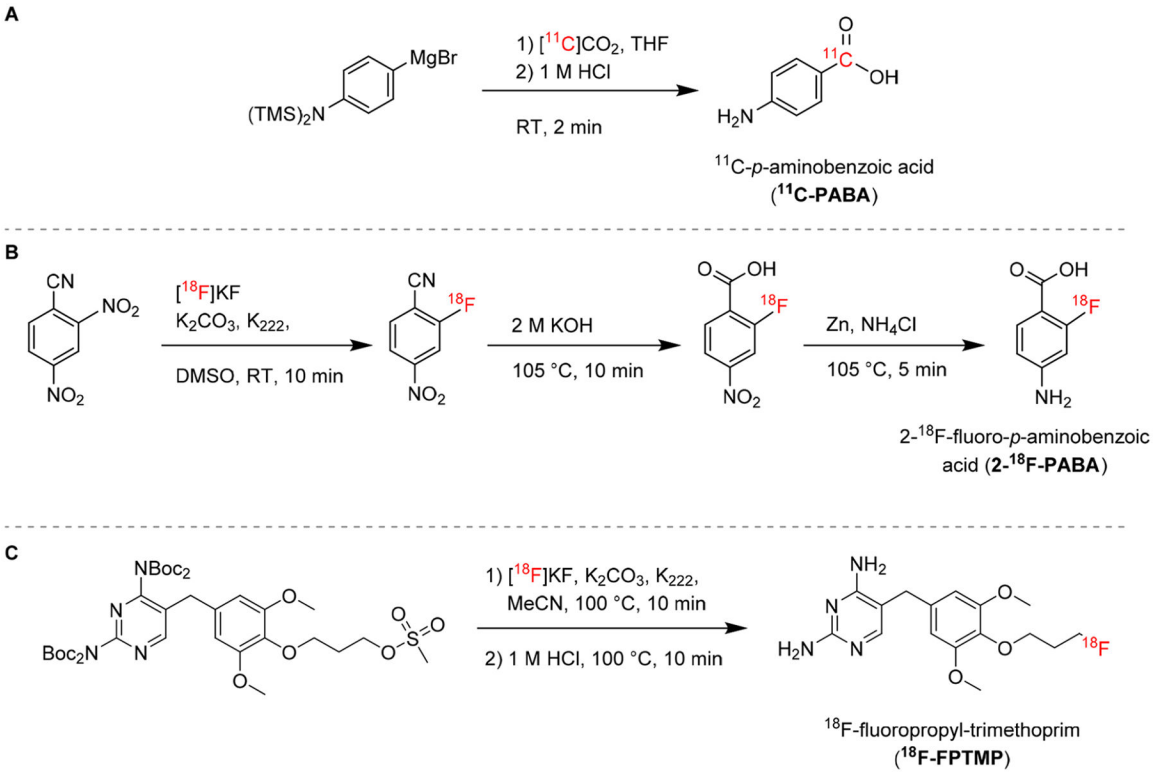

Figure 3.

Radiosynthesis of radiotracers based on folate metabolism. (A) ^{11}C-PABA is prepared by nucleophilic addition of a Grignard reagent to cyclotron-generated $^{11}CO_2$[32]. (B) 2-^{18}F-PABA can be prepared in three steps by nucleophilic aromatic substitution with ^{18}F-fluoride, followed by hydrolysis of a nitrile to carboxylic acid, and reduction of a nitro group to a primary amine.[15] (C) ^{18}F-FPTMP is radiolabeled in a one-pot two-step reaction by nucleophilic substitution of the boc-protected mesylate precursor followed by acidic deprotection.16

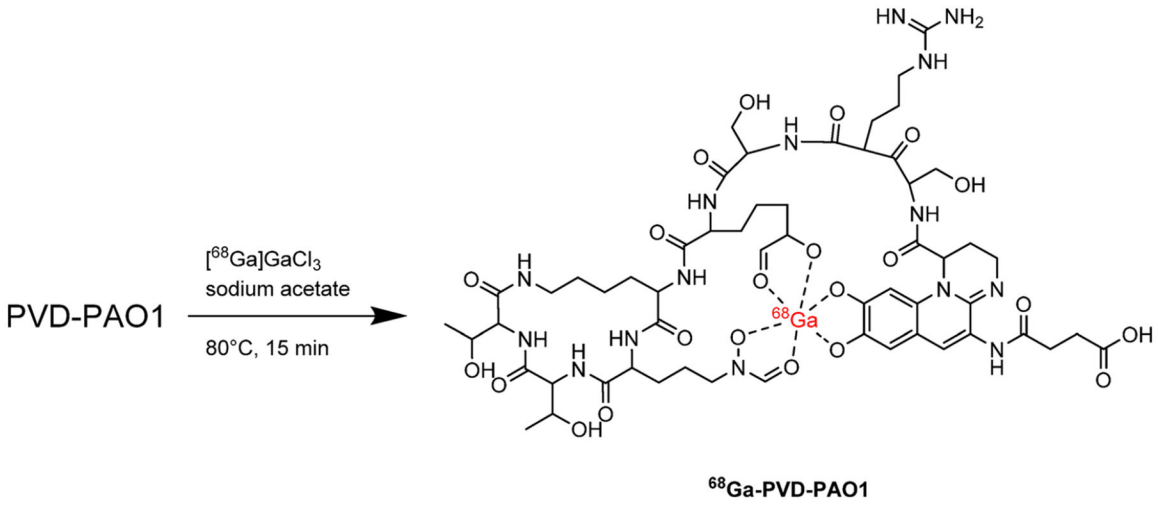

Figure 4.

Radiosynthesis of ^{68}Ga-siderophores for imaging of bacterial iron metabolism: ^{68}Ga-PVD–PAO1 is prepared by generator-produced ^{68}Ga in the form of ^{68}Ga-gallium citrate in aqueous solution.17

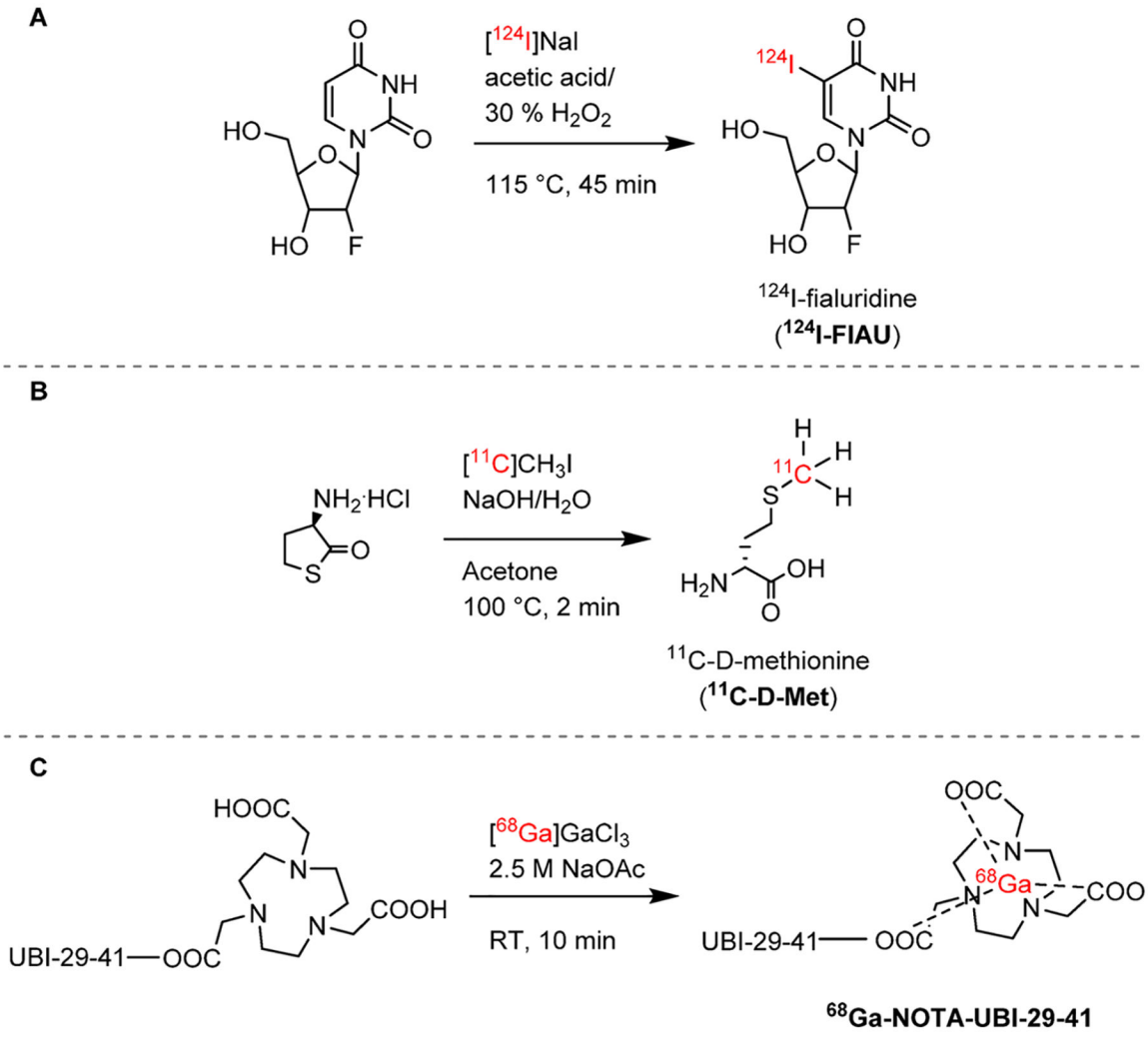

Figure 5.

Radiosynthesis of nucleic acid^{124}I-FIAU and radiotracers targeting bacterial cell wall components and intracellular proteins. (A) ^{124}I-FIAU is obtained by radioiodination of 1-(2′-deoxy-1-β-D-arabinofuranosyl)-uracil.[37] (B) ^{11}C-D-Met is radiolabeled by methylation of D-homocysteinethiolactone.[20] (C) ^{68}Ga-NOTA–UBI-29–41 is obtained by chelation of ^{68}Ga using a NOTA ligand attached the peptide.22

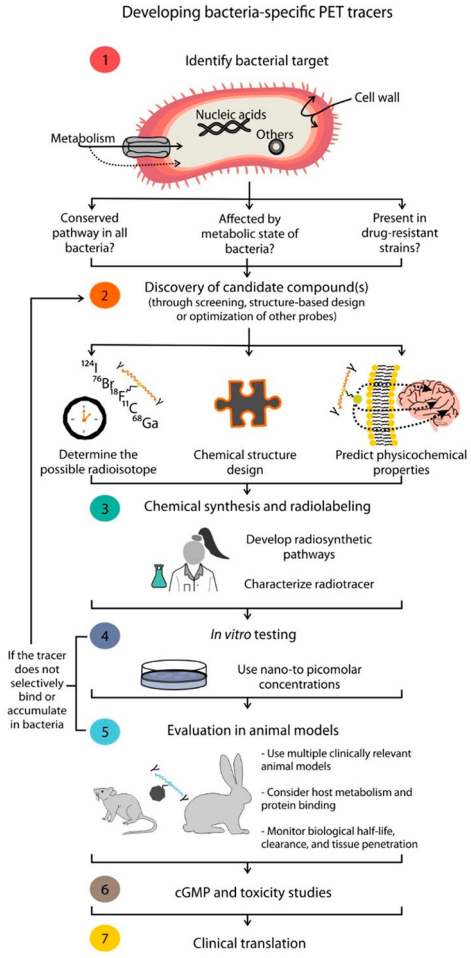

Figure 6.
Considerations for the design and development of pathogen-specific PET imaging agents.

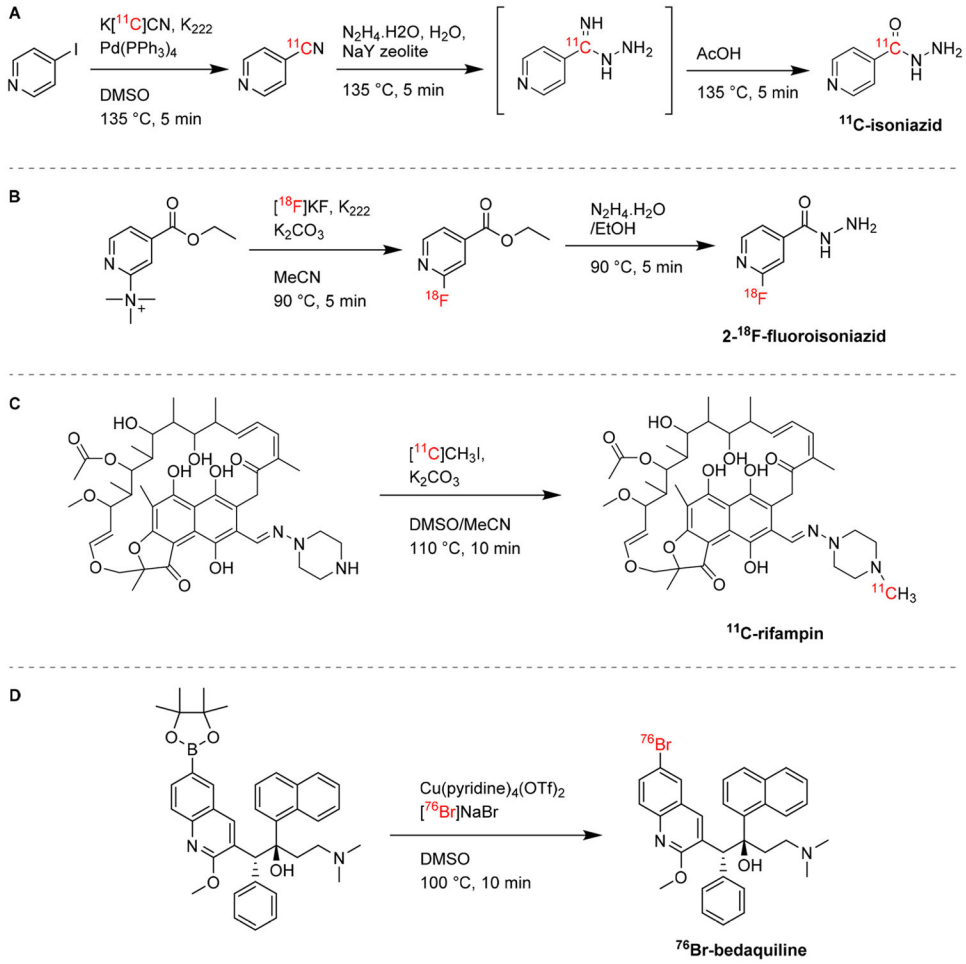

Figure 7.

Radiosynthesis of antimycobacterials and analogues. (A) ^{11}C-Isoniazid is obtained by treating iodopyridine with ^{11}C-HCN to generate ^{11}C-cyanopyridine, which is then converted into a hydrazine by nucleophilic attack and subsequently hydrolyzed, in a three-step one-pot reaction.[49](B) 2-^{18}F-Fluoroisoniazide is radiolabeled by ^{18}F nucleophilic substitution on an ammonium-leaving group through the intermediate ^{18}F-fluoroisonicotiate.[50] (C) ^{11}C-Rifampin can be radiolabeled through *N*-methylation with $^{11}CH_3I$.[49] (D) ^{76}Br-Bedaquiline is obtained by copper-mediated nucleophilic radiobromination of the boronic pinacol ester precursor.57

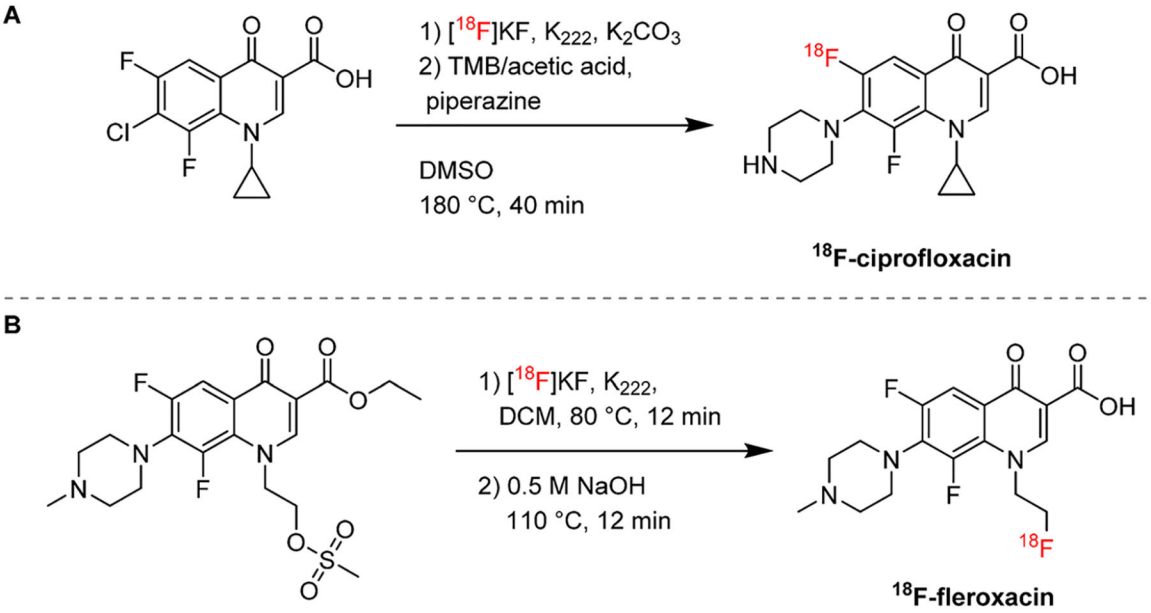

Figure 8.

Radiosynthetic strategies for fluoroquinolones. (A) ^{18}F-Ciprofloxacin can be radiolabeled through ^{19}F–^{18}F-isotopic exchange in two steps.[65] (B) ^{18}F-Fleroxacin is obtained through ^{18}F nucleophilic substitution of a mesylate precursor.66

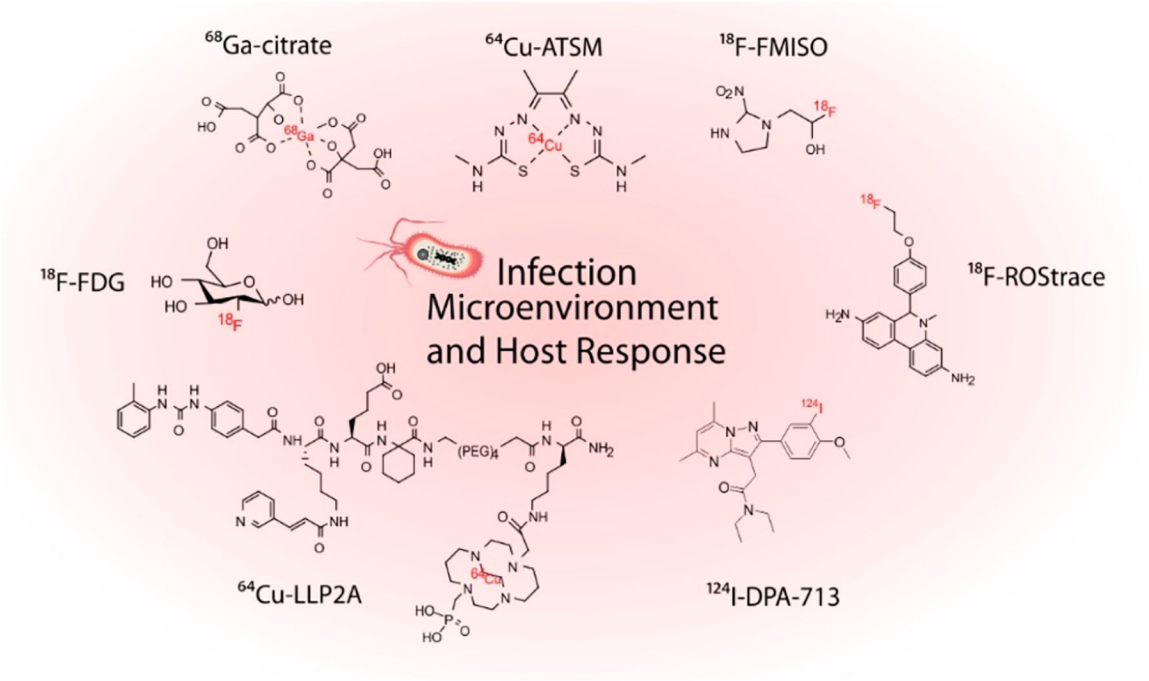

Figure 9.
Chemical structures of selected radiotracers used for PET imaging of the host response at infection sites.

Table 1.

Pathogen-Specific Radiotracers: Uptake Mechanism and Biological Findings

tracer	mechanism of bacterial uptake	preclinical or clinical findings	therapeutic monitoring and rapid detection of MDR bacteria
^{18}F-FDS	Metabolized selectively by Enterobacteriales (*Escherichia coli, Klebsiella* sp., *Enterobacter* sp., *Salmonella* sp., etc.)	Able to distinguish infection from sterile inflammation in animals.[8] Tested in healthy humans with favorable dosimetry as well as promising results in a cohort of infected patients.[9,10]	Sequential ^{18}F-FDS PET scan before and after antibiotic therapy could rapidly detect therapeutic failures associated with MDR, extended-spectrum β-lactamase (ESBL)-producing *E. coli* (clinical strain) in mice.[8]
^{18}F-maltodextrin	Maltose–maltodextrin transporter functional in metabolically active bacteria.	Animal studies to detect infection.[11]	Sequential ^{18}F-maltodextrin PET scan before and after antibiotic therapy could measure efficacy in a rat model of *E. coli* infection.[11]
6″-^{18}F-fluoromaltotriose	Maltose–maltodextrin transporter functional in metabolically active bacteria	Able to distinguish infection from sterile inflammation in animals.[12]	6″-^{18}F-fluoromaltotriose PET signal disappeared after 1 month of antibiotic therapy in a rat model of *S. aureus* infection.[12]
^{11}C-PABA	Substrate for bacterial de novo synthesis of folic acid	Distinguishes infection from sterile inflammation in a myositis animal model.[13] Preliminary testing in healthy humans with favorable dosimetry.[14]	
2-^{18}F-PABA	Substrate for bacterial de novo synthesis of folic acid	Distinguishes infection from sterile inflammation in a myositis animal model.[15]	Sequential 2-^{18}F-PABA PET scan before and after antibiotic therapy could rapidly detect therapeutic failures associated with MDR *S. aureus* in mice.[15]
^{18}F-FPTMP	Binds and inhibits bacterial dihydrofolate reductase	Increased uptake in infected tissue compared to sterile inflammation or cancer (breast carcinoma) in small animal models. Low retention in nontarget organs in nonhuman primates.[16]	
^{68}Ga-PVD-PAO1	Bacterial siderophore FpvA transporter	Detects infection in lung and myositis animal models.[17]	
^{124}I-FIAU	Bacterial thymidine kinase	Clinical studies show low specificity in patients with suspected prosthetic joint infections.[18,19]	
^{11}C-D-Met	Incorporated into the bacterial cell wall	Distinguishes infection from sterile inflammation in small animals.[20,21]	
^{68}Ga-NOTA-UBI-29–41	Targets the bacterial cell wall	Increased uptake in infected tissue compared to sterile inflammation in small animals.[22] Case-reports and case-series of human use.[23,24]	Sequential ^{99m}Tc-UBI 29–41 scintigraphy before and after antibiotic therapy correlated with clinical outcomes in a patient cohort.[25]